J Mater Sci: Mater Med (2010) 21:1225–1232
DOI 10.1007/s10856-009-3982-z

Sensing of protein adsorption with a porous bulk composite comprising silver nanoparticles deposited on hydroxyapatite

Chikara Ohtsuki · Yuji Ichikawa · Hiroyuki Shibata · Giichiro Kawachi · Tsukasa Torimoto · Shin-ichi Ogata

Received: 12 September 2009 / Accepted: 23 December 2009 / Published online: 6 January 2010

Abstract Porous bulk composites were produced by depositing silver nanoparticles of diameter 11.0 ± 3.2 nm on hydroxyapatite of micrometer sizes. Adsorption of bovine serum albumin (BSA) and lysozyme (LSZ) on the composite material was observed in 2 and 10 mol m^{-3} phosphate buffer solutions. More BSA than LSZ was adsorbed in 2 mol m^{-3} phosphate buffer and this was attributed to a larger *a*-face surface area present in the plate- and rod-shaped hydroxyapatite compared with the *c*-face surface area. Peak shifts in localized surface plasmon resonance (LSPR) spectra were clearly related to adsorbed amounts of BSA and LSZ after exposure of the porous bulk composites to protein solutions. The sensing capability of the porous bulk composite results from changes in the dielectric constant of the surface fluid surrounding the silver nanoparticles. Adsorption/desorption cycles of BSA were applied to the porous bulk composite, confirming the reversibility of the sensing capability.

1 Introduction

Silver nanoparticles have a sensing capability derived from localized surface plasmon resonance (LSPR), which is an optical feature of noble metal nanoparticles [1–4]. Hydroxyapatite (HAp, $Ca_{10}(PO_4)_6(OH)_2$) has been reported to show specific adsorption characteristics for proteins, caused by the surface electric charge on the hydroxyapatite, as well as osteoconductive properties [5–8]. Thus, the combination of the functions derived from silver nanoparticles and hydroxyapatite can produce a sensor material that has specific adsorption properties for proteins and a bioactivity suitable for artificial bone. Recently, we reported a fabrication process for composites comprised of silver nanoparticles deposited on hydroxyapatite crystals, through reduction of Ag^+ ions in a slurry containing hydroxyapatite particles [9]. The composite structure incorporated silver nanoparticles of approximately 12 nm in diameter on the surface of the hydroxyapatite. The hybridization was successful even when free from surfactant, maintaining similar characteristics to plain hydroxyapatite.

Behavior of protein adsorption on hydroxyapatite depends on the morphology of their crystals, where the *a*- and *c*-faces are positively and negatively charged, respectively, under physiological conditions (around pH 7.4). Actually, the specific morphology of hydroxyapatite leads to unique characteristics for adsorption of proteins [10]. It is therefore worth developing composites of silver nanoparticles with hydroxyapatite substrates with designed morphology.

The present study is focused on fabrication on porous bulk composites consisting of hydroxyapatite modified with silver nanoparticles, to investigate the capability for sensing protein adsorption. Porous bulk composites were prepared for convenient availability of the composite during the investigation into protein adsorption. Porous bulk specimens consisting of micrometer-sized hydroxyapatite were prepared by hydrothermal processing of powder compacts of alpha-tricalcium phosphate (α-TCP, $Ca_3(PO_4)_2$), according

C. Ohtsuki (✉) · Y. Ichikawa · H. Shibata · G. Kawachi · T. Torimoto
Graduate School of Engineering, Nagoya University, Furo-cho, Chikusa-ku, Nagoya 464-8603, Japan
e-mail: ohtsuki@apchem.nagoya-u.ac.jp

S. Ogata
Graduate School of Environment and Information Science, Yokohama National University, 79-7, Tokiwadai, Hodogaya-ku, Yokohama 240-8501, Japan

to a previous report [11]. For evaluation of protein adsorption, bovine serum albumin (BSA) and lysozyme (LSZ) were used in the phosphate buffer solution at a phosphate concentration of 2 or 10 mol m^{-3}. To detect the concentration of protein adsorbed on the rod-shaped hydroxyapatite, peak shifts in LSPR spectra were measured. Moreover, the cyclic process of adsorption and desorption of BSA on the porous bulk composites was evaluated.

2 Experimental procedures

2.1 Preparation of silver nanoparticles/hydroxyapatite composites

Figure 1 shows the procedure for synthesis of porous bulk composites consisting of micrometer-sized hydroxyapatite and their modification with silver nanoparticles. The hydroxyapatite was prepared using a hydrothermal processing route according to a method obtained from the literature [11]. 0.4 g of α-TCP (Taihei Chemical Industrial Co. Ltd., Osaka, Japan) powder was compacted by a uniaxial press (Shimadzu Co., Kyoto, Japan) at 124 MPa to form a pellet 12 mm in diameter. The α-TCP pellet was hydrothermally treated in a designed vessel (Shikokurika Co., Ltd, Kochi, Japan). Specimens of the compacted powder were placed in 30 cm^3 of ultrapure water at a temperature of 120°C for a period of 3 h in an autoclave (100 cm^3). The specimen was then washed with ultrapure water for a period of 15 min, followed by drying at 100°C in air for more than 12 h. The product was shown to be hydroxyapatite by powder X-ray diffraction measurements.

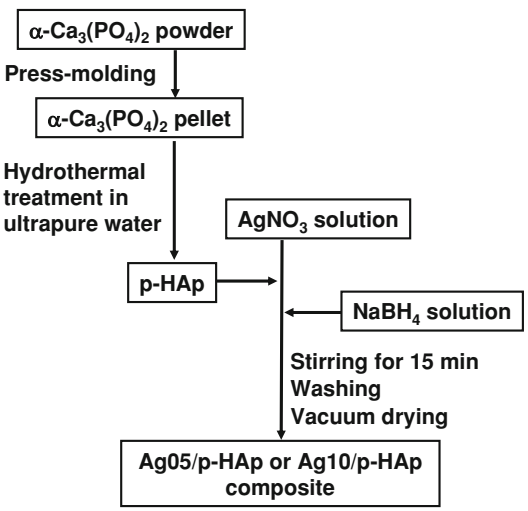

Fig. 1 Procedure for the synthesis of rod-shaped hydroxyapatite materials and their modification with silver nanoparticles

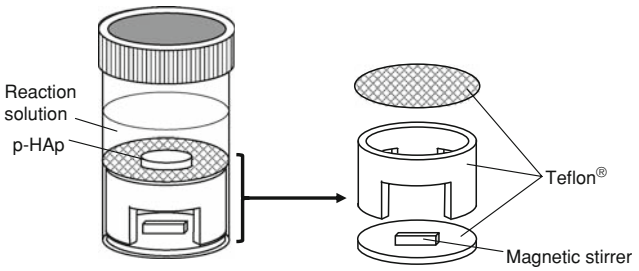

Fig. 2 Apparatus for modification of rod-shaped hydroxyapatite blocks with silver nanoparticles

Deposition of silver nanoparticles on the hydroxyapatite was performed by reduction of silver nitrate ($AgNO_3$, Kishida Chemical Co. Ltd, Osaka, Japan) using sodium tetrahydroborate ($NaBH_4$, Kishida Chemical Co. Ltd) in a polystyrene bottle as shown in Fig. 2. An appropriate amount of $AgNO_3$ was dissolved in 20 cm^3 of ultrapure water to prepare the Ag^+ solution at a concentration of 0.5 or 1.0 mmol cm^{-3}. The porous bulk hydroxyapatite was then immersed in the silver nitrate solution. 0.2 cm^3 of $NaBH_4$ solution was then added to the solution under stirring to give a molar ratio of $AgNO_3/NaBH_4 = 1/5$. The porous bulk composites formed a yellow color within a few minutes. After the solution was stirred at room temperature for a further 15 min, the composite product was removed from the solution and washed with ultrapure water, followed by vacuum drying at room temperature for more than 12 h. Finally, a yellow-colored bulk composite was obtained. The materials synthesized using solutions with Ag^+ concentrations of 0.5 and 1.0 mmol cm^{-3} are hereafter abbreviated "Ag05/p-HAp" and "Ag10/p-HAp", respectively. Porous bulk hydroxyapatite without silver nanoparticles is abbreviated "p-HAp".

The bulk specimens obtained were ground by a mortar for characterization by X-ray diffraction (XRD; RINT PC2100, Rigaku Co., Tokyo, Japan) using CuKα radiation, measurement of surface area by the BET method with N_2 as the adsorbate (NOVA 1000e, Yuasa Ionics Co. Ltd, Osaka, Japan) and observation by scanning electron microscope (SEM; JMS5600, JEOL Ltd, Tokyo, Japan) and transmission electron microscope (TEM; H-800, Hitachi Ltd, Tokyo, Japan) with an acceleration voltage of 200 kV. The Ca/P atomic compositions of the hydroxyapatite crystals in the specimens were determined using inductively coupled plasma emission spectroscopy (ICP-AES; Optima 2000 DV, PerkinElmer Japan Co. Ltd, Yokohama, Japan) following dissolution of the powder in a 10 vol.% nitric acid solution with a ratio of powder/solution = 1 mg/20 cm^3. The diffuse reflectance spectra of the specimens were measured using ultraviolet-visible (UV-vis) spectrophotometer (V-560,

JASCO Co., Tokyo, Japan) with an integration sphere attachment to characterize the silver nanoparticles by Kubelka–Munk functions.

2.2 Protein adsorption on the silver nanoparticles/hydroxyapatite composites

Phosphate buffer solutions of 2 or 10 mol m^{-3} were prepared by dissolving sodium dihydrogen phosphate dihydrate ($NaH_2PO_4 \cdot 2H_2O$, Nacalai Tesque Inc., Kyoto, Japan) and disodium hydrogen phosphate 12hydrate ($Na_2HPO_4 \cdot 12H_2O$, Nacalai Tesque Inc.) at pH 7.4. Proteins were each dissolved in the phosphate buffer to a concentration of 0.8 mg cm^{-3}. Two types of proteins were used: bovine serum albumin (BSA; Wako Pure Chemical Industries, Ltd., Osaka, Japan) as a model acidic protein and lysozyme (LSZ; Wako Pure Chemical Industries, Ltd.) as a model basic protein.

A pellet of the porous bulk specimen p-HAp or Ag05/p-HAp was placed in 2.0 cm^3 of the protein solutions. After soaking at 37°C, 0.02 cm^3 of the solution was extracted from the supernatant to determine the concentration of the proteins by Bradford assay, using a BioRad protein assay kit (Bio-Rad Laboratories Inc., Tokyo, Japan). Absorption at 595 nm was measured by ultraviolet-visible (UV-vis) spectrometer (U-3410, Hitachi Ltd.), by standard curves made for corresponding proteins. The accuracy on the determination of protein adsorption was estimated to be percentage errors of less than 6% both for BSA and LSZ, based on preliminary examination determining adsorption amounts per unit area (mg m^{-2}) by triplicate measurement for each samples under similar condition using powder of silver nanoparticles/hydroxyapatite composites. Also, the diffuse reflectance spectra of the specimens were measured before and after exposure to the protein solutions for 60 h using a UV-vis spectrophotometer (V-560, JASCO Co.) with an integration sphere attachment. In the measurements of the diffuse reflectance spectra, pure barium sulfate (Nacalai Tesque Inc.) was used as a reference, while samples were diluted with barium sulfate to give a content of 50 vol.%.

2.3 LSPR spectra of the composite with cyclic protein adsorption and desorption

The LSPR spectra of Ag05/p-HAp were measured through cyclic adsorption and desorption of BSA. The Kubelka–Munk functions of the soaked specimen were obtained after normalization to evaluate the peak shifts in the LSPR spectra of the dried specimens, as well as the concentration of proteins in the solution after contact with Ag05/p-HAp. Steps given in Table 1 were chosen for measurement.

3 Results

3.1 Structure of silver nanoparticles/hydroxyapatite composites

Figure 3 shows powder X-ray diffraction patterns for samples of p-HAp, Ag05/p-HAp and Ag10/p-HAp. The crystalline phase in the composite products was identified as hydroxyapatite. The XRD pattern of Ag10/p-HAp shows trace amounts of silver at about $2\theta = 38.1°$. Figure 4 shows SEM photographs of p-HAp, Ag05/p-HAp and Ag10/p-HAp. Plate- and rod-shaped crystals were observed on all the photographs, irrespective of the type of sample. Figure 5 shows TEM photographs of p-HAp, Ag05/p-HAp and Ag10/p-HAp. TEM observation revealed that Ag05/p-HAp and Ag10/p-HAp had small particles on the plate- and rod-shaped crystals, whereas p-HAp did not. The mean diameters of Ag05/p-HAp and Ag10/p-HAp were 7.9 and 11.0 nm, respectively, after a count of at least 200 particles on the photographs. There seems to be no significant difference in the shapes of the crystals between p-HAp and the specimens after modification with silver nanoparticles, i.e., Ag05/p-HAp and Ag10/p-HAp. Figure 6 shows diffuse reflectance spectra and its Kubelka–Munk function for synthesized specimens of p-HAp, Ag05/p-HAp and Ag10/p-HAp. After hybridization with silver nanoparticles, a distinct peak was detected at a wavelength of around 400 nm in the LSPR

Table 1 Steps for examination of adsorption and desorption of BSA

Step	Condition	Treatment
(1)	Before soaking	After synthesis of Ag05/p-HAp,
(2)	After first adsorption	Soaking the Ag05/p-HAp in the solution containing BSA at a concentration of 0.8 mg cm^{-3} with 10 mol m^{-3} phosphate for 3 h at 37°C.
(3)	After first desorption	Following (2), the specimen of Ag05/p-HAp was soaked in buffer solution free from protein with a phosphate concentration of 200 mol m^{-3} for 3 h at 37°C.
(4)	After second desorption	Following (3), the specimen of Ag05/p-HAp was soaked in buffer solution free from protein with a phosphate concentration of 200 mol m^{-3} for another for 3 h at 37°C.
(5)	After second adsorption	Following (4), the Ag05/p-HAp was soaked again in a solution containing BSA at a concentration of 0.8 mg cm^{-3} with 10 mol m^{-3} phosphate for 3 h at 37°C.

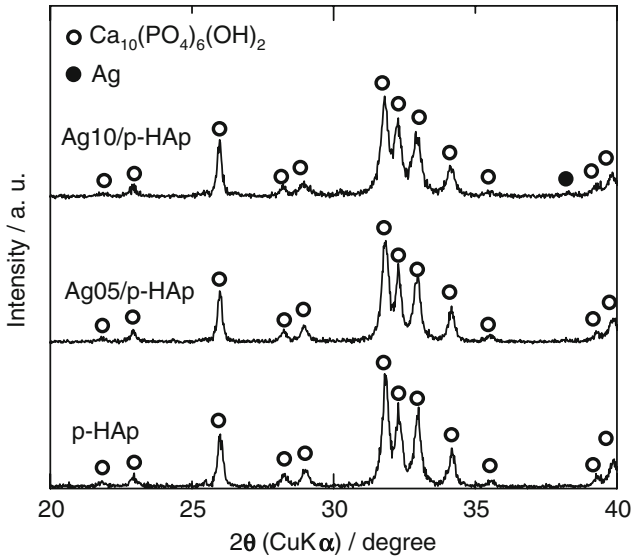

Fig. 3 Powder X-ray diffraction patterns of samples of p-HAp, Ag05/p-HAp and Ag10/p-HAp

spectra. The LSPR showed a peak typically around 400 nm in wavelength, dependent of the concentration of the deposited silver nanoparticles. Ag10/p-HAp showed a higher peak intensity for the Kubelka–Munk function than Ag05/p-HAp. The characteristics of the synthesized specimens p-HAp, Ag05/p-HAp and Ag10/p-HAp are summarized in Table 2, including Ca/P atomic ratio and specific surface area. While the Ca/P atomic ratios were below the value of stoichiometric, 1.67, HAp was obtained, and there were no significant differences in hydroxyapatite among the specimens, p-HAp, Ag05/p-HAp and Ag10/p-HAp.

3.2 Protein adsorption behavior on the composites and its LSPR spectra

Figure 7 shows changes in protein concentrations in the 2 mol m^{-3} phosphate solution due to immersion of Ag05/p-HAp. "Blank" indicates the solution without immersion of Ag05/p-HAp. There was typically a decrease in BSA concentration after immersion of Ag05/p-HAp. Note that the degree of the decrease in BSA was much larger than that for LSZ. This indicates that the adsorption capability for LSZ was small. The adsorptions of BSA and LSZ were also observed in the 10 mol m^{-3} phosphate buffer solution, as shown in Fig. 8. Figure 9 shows Kubelka–Munk functions for Ag05/p-HAp before soaking (0 h) and after soaking in the 2 mol m^{-3} phosphate buffer solutions for 60 h. Figure 10 shows Kubelka–Munk functions of Ag05/p-HAp before soaking (0 h) and after soaking in the 10 mol m^{-3} phosphate buffer solutions for 60 h. The peak shifts in the LSPR spectra of Ag05/p-HAp can be clearly

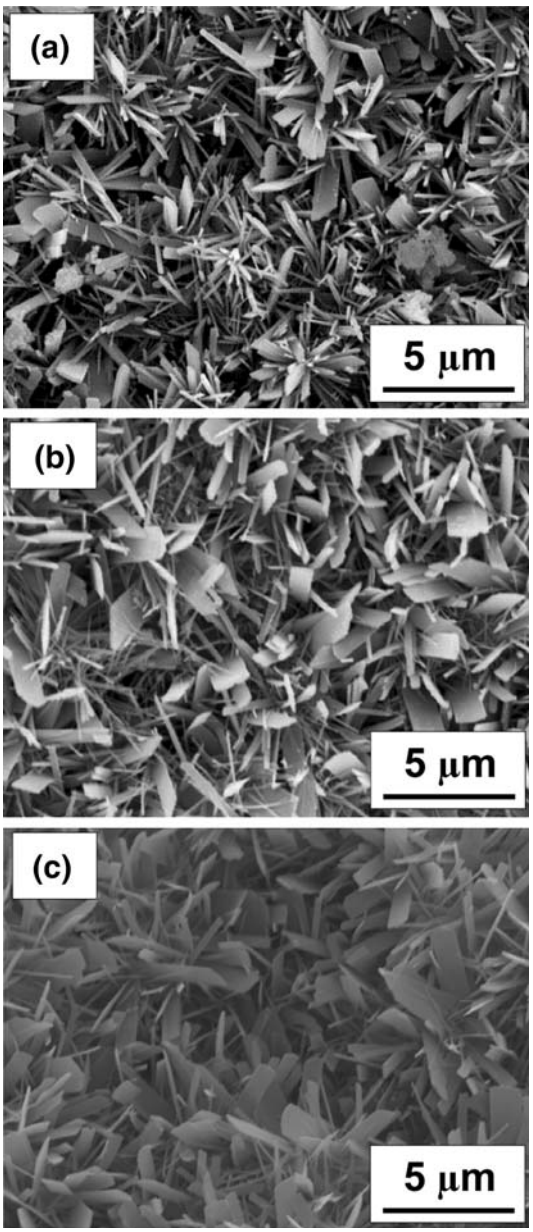

Fig. 4 SEM photographs of (**a**) p-HAp, (**b**) Ag05/p-HAp and (**c**) Ag10/p-HAp

observed for both the 2 and 10 mol m^{-3} phosphate buffer solutions, irrespective of protein type, whereas there appears to be no shift in the peaks after exposure to the protein-free solution.

3.3 LSPR spectra of the composite after cyclic protein adsorption and desorption

Figure 11 shows the Kubelka–Munk function for Ag05/p-HAp after repeated cycles of adsorption and desorption of BSA. There is an obvious relationship between the peak shifts and the adsorbed amounts of proteins as estimated by

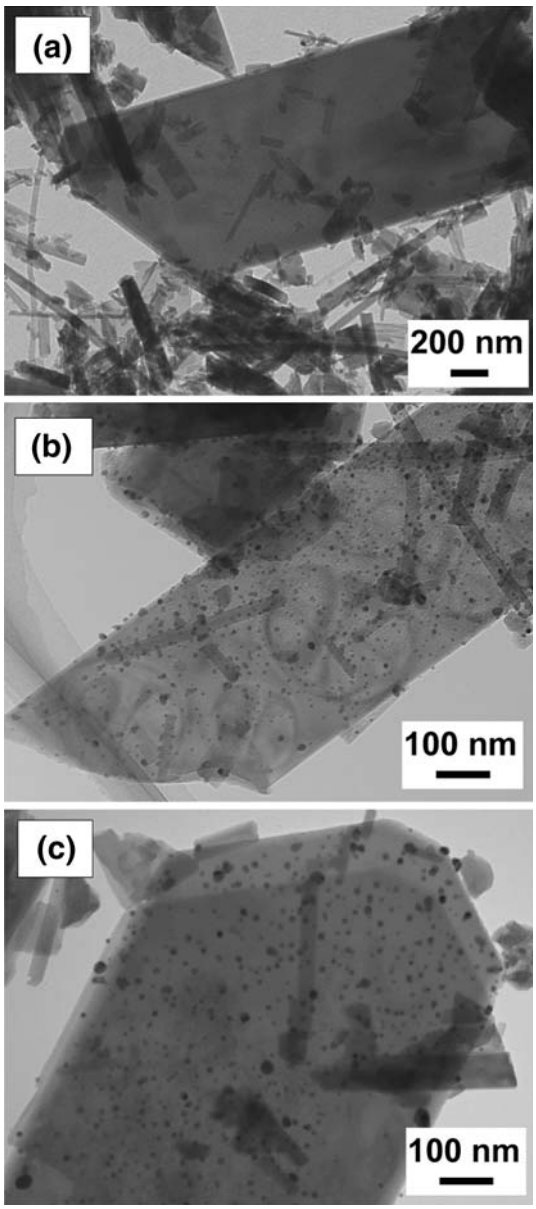

Fig. 5 TEM photographs of (**a**) p-HAp, (**b**) Ag05/p-HAp and (**c**) Ag10/p-HAp

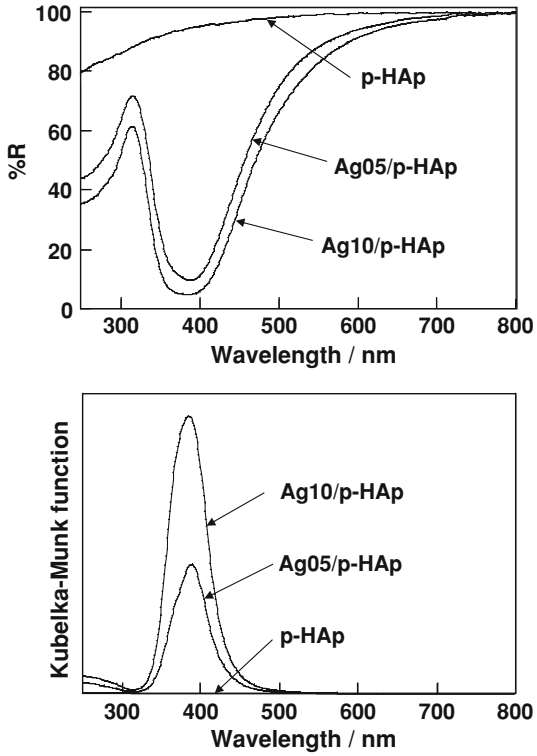

Fig. 6 Diffuse reflectance spectra (upper) and its Kubelka–Munk function (lower) for specimens of p-HAp, Ag05/p-HAp and Ag10/p-HAp

the measurement of the protein concentration after exposure of the composite to the solutions.

4 Discussion

The present study indicates successful preparation of porous bulk composites consisting of plate- and rod-shaped hydroxyapatite with modification by silver nanoparticles. After preparation, the amounts of silver nanoparticles incorporated depended on the initial concentrations of the starting materials.

After soaking Ag05/p-HAp, a decrease in protein concentration was detected for BSA and LSZ. This decrease is attributed to protein adsorption on the hydroxyapatite surface. A lower amount of LSZ than BSA was adsorbed at a phosphate concentration of 2 mol m^{-3}. The plate- and rod-shaped hydroxyapatite crystals have only a small negatively charged *c*-face area that allows interaction with positively charged species at pH 7.4. The BSA would be negatively charged, while LSZ would be positively charged. At the lower concentration of phosphate, LSZ could not be adsorbed on the *a*-face, thus less adsorption of LSZ occurred. At the higher phosphate concentration, negatively charged phosphate ions would react with the *a*-face to result in a relatively low degree of positive charge and increase the amount of adsorbed protein. The amounts of adsorbed protein were well-related to the peak shift in LSPR spectra for both 2 and 10 mol m^{-3} buffer solutions. The peak shift was caused by changes in the dielectric constant around the silver nanoparticles.

Peak shifts in LSPR were detected and correlated well with the amount of protein adsorption on the hydroxyapatite surfaces. Silver nanoparticles typically show absorption spectra due to LSPR. As reported previously, the wavelength of absorption is generally understood by the following equation [4, 12] on the basis of Mie's theory

Table 2 Characteristics of specimens

Characteristics	Sample name		
	p-HAp	Ag05/p-HAp	Ag10/p-HAp
Ca/P atomic ratio	1.58	1.58	1.58
Specific surface area	14.4 $m^2\ g^{-1}$	13.3 $m^2\ g^{-1}$	14.9 $m^2\ g^{-1}$
Size of silver nanoparticles (mean ± SD)	nd	7.9 ± 2.6 nm	11.0 ± 3.2 nm

nd not determined

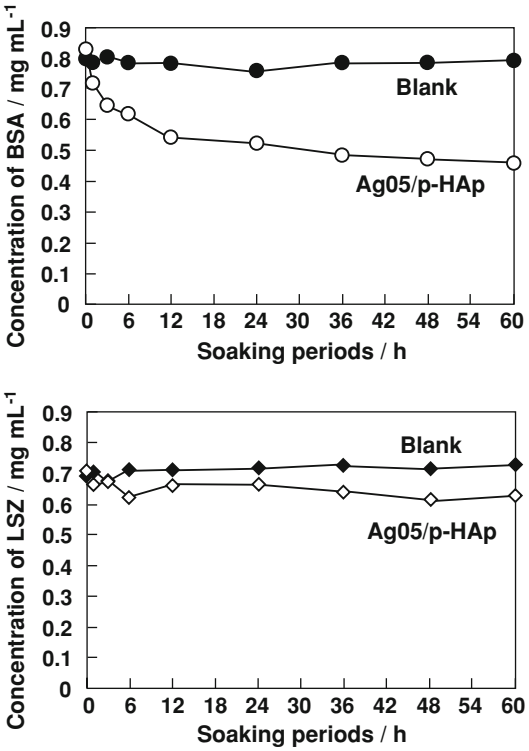

Fig. 7 Changes in protein concentrations in a 2 mol m^{-3} phosphate concentration due to immersion of Ag05/p-HAp

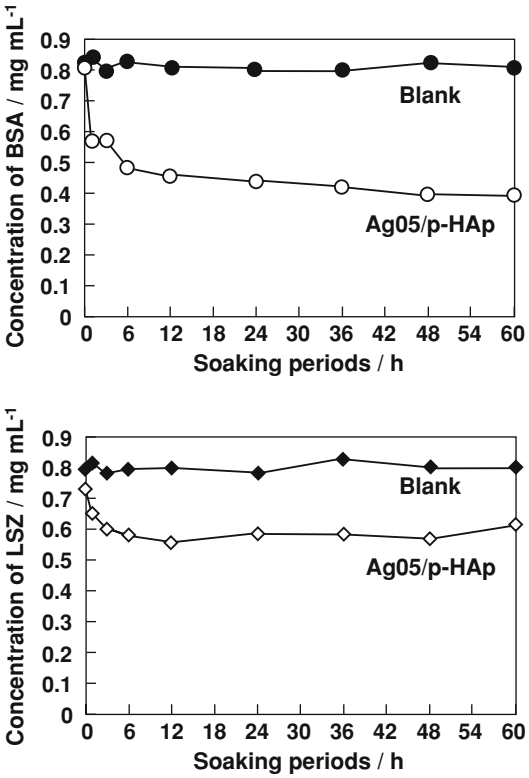

Fig. 8 Changes in protein concentrations in a 10 mol m^{-3} phosphate concentration due to immersion of Ag05/p-HAp

$$E(\lambda) = \frac{24\pi N_A a^3 \varepsilon_m^{\frac{3}{2}}}{\lambda \cdot \ln(10)} \left[\frac{\varepsilon_i}{(\varepsilon_r + v\varepsilon_m)^2 + \varepsilon_i^2} \right] \quad (1)$$

where E(λ) is the extinction (viz., the sum of absorption and scattering), N_A is the areal density of nanoparticles, a is the radius of the metallic nanosphere, ε_m is the dielectric constant of the medium surrounding the metallic nanosphere (assumed to be a positive, real number and wavelength independent), λ is the wavelength of the absorbing radiation, ε_i is the imaginary portion of the metallic nanoparticle's dielectric function, ε_r is the real portion of the metallic nanoparticle's dielectric function and v is a term that describes the aspect ratio of the nanoparticle ($v = 2$ for a sphere). From Eq. 1, it can be seen that LSPR spectra are affected by the size, shape, composition and distribution of the nanoparticles, which are determined by the synthesis process. These parameters are not expected to change during protein adsorption on the hydroxyapatite in the composites. In contrast, protein adsorption leads to changes in the dielectric constant around the nanoparticles. The changes in the dielectric constant around the nanoparticles then results in a peak shift in the LSPR spectra. Sizes of BSA and LSZ are reported to be 14 × 4 × 4.5 nm^3 and 4.5 × 3 × 3 nm [3, 13], which are comparable with the sizes of the silver nanoparticles deposited on the hydroxyapatite substrate. The surface coverage area of silver nanoparticles on the hydroxyapatite substrate is quite small compared with the total surface area of the substrate. The peak shifts in the LSPR spectra were therefore attributed to changes in the dielectric constant around the surface of the silver nanoparticles due to adsorption of proteins on hydroxyapatite in the vicinity of the nanoparticles. The peak shifts are related to the

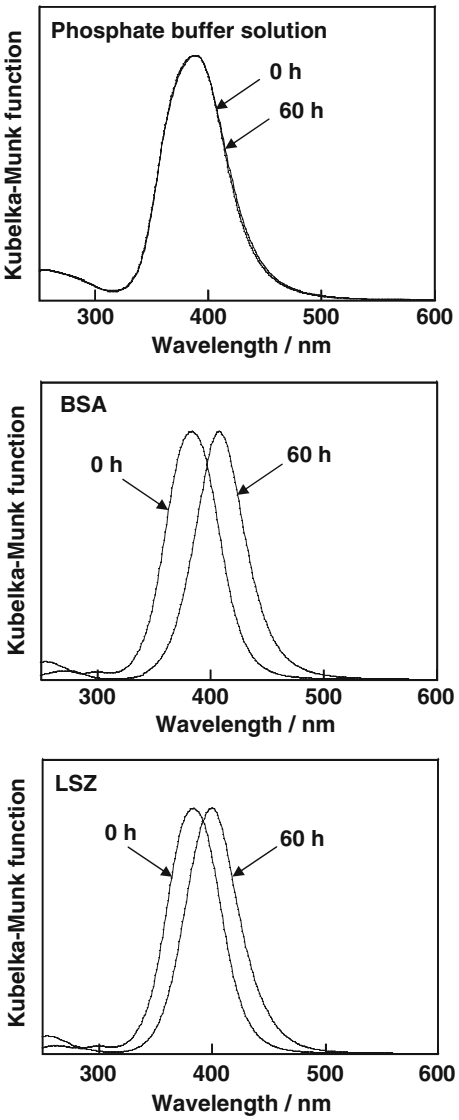

Fig. 9 Kubelka–Munk functions of Ag05/p-HAp before soaking (0 h) and after soaking in buffer solutions at a phosphate concentration of 2 mol m^{-3} for 60 h

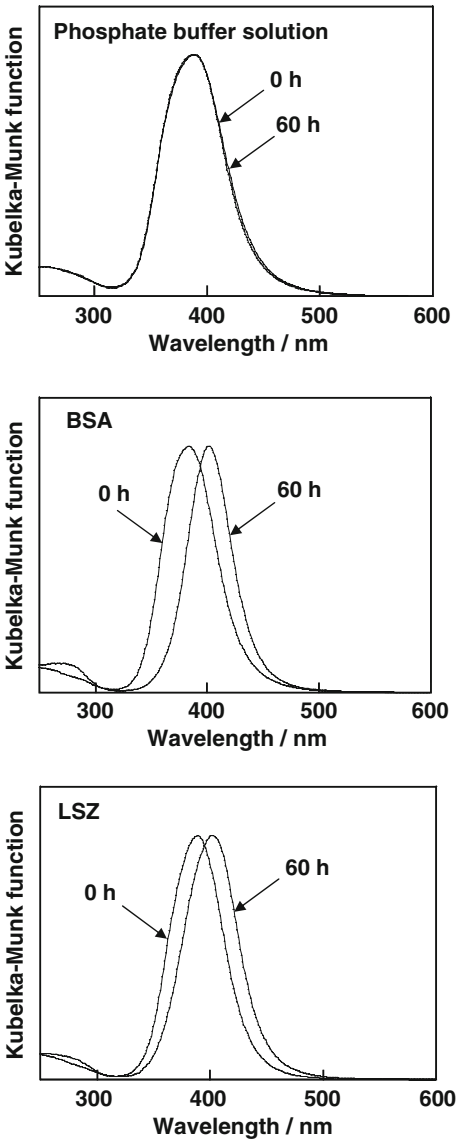

Fig. 10 Kubelka–Munk functions of Ag05/p-HAp before soaking (0 h) and after soaking in a buffer solution at a phosphate concentration of 10 mol m^{-3} for 60 h

concentration of nanoparticles in the regions where proteins exist near the surface of the nanoparticles and therefore the peak shifts mainly exhibit the adsorption of proteins on the *a*-face surface that is predominant in the hydroxyapatite prepared in this study. Further selectivity between acidic and basic protein adsorption is expected with fabrication of alternative morphologies, such as needles [10]. Furthermore, effects of amount of silver nanoparticles on the hydroxyapatite substrates is required as future works, while we evaluate the sensing property of proteins on the samples with lower amounts of silver nanoparticles in the present study.

An adsorption and desorption cycle was also observed to correspond with the amount of protein in the vicinity of silver nanoparticles. Removal of BSA after adsorption could be achieved using a high phosphate concentration. A single desorption step was not sufficient to completely desorb the protein but a second desorption step removed almost all of the protein. The silver nanoparticle/hydroxyapatite composites reversibly adsorbed proteins and protein adsorption results could all be related to peak shifts in LSPR spectra. There is therefore potential for creating new materials for sensing protein adsorption, using the characteristics of hydroxyapatite.

5 Conclusions

The protein adsorption sensing capabilities of porous bulk composites consisting of silver nanoparticles and

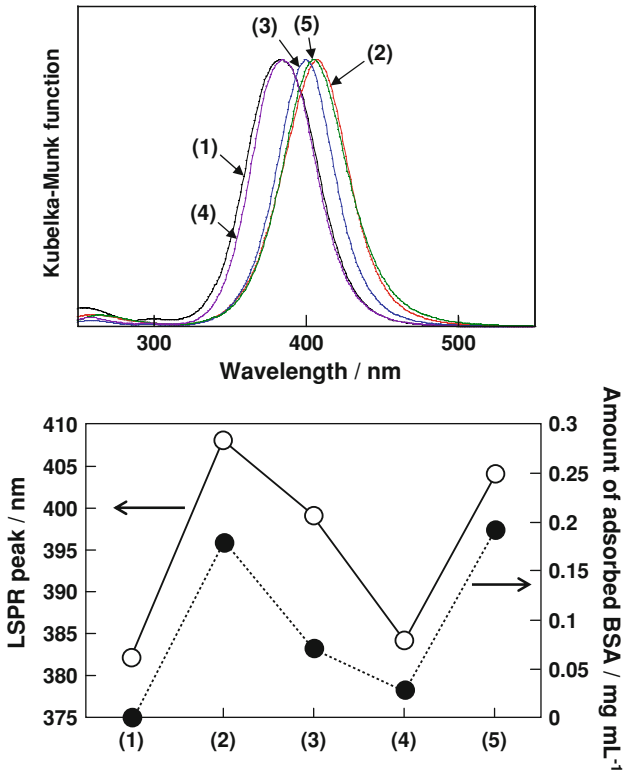

Fig. 11 Kubelka–Munk function of Ag05/p-HAp after cyclic adsorption and desorption of BSA

hydroxyapatite were determined by measuring the relationships between changes in protein concentration and peak shifts in LSPR spectra. The adsorption behavior of the composites showed dependence on the crystalline morphology of the hydroxyapatite that would provide adsorption sites due to surface charges on the exposed face. The peak shift due to adsorption of the proteins was clearly reversible after desorption of the protein. The silver nanoparticles and hydroxyapatite composites are promising candidates for sensing materials that can detect protein adsorption and desorption.

Acknowledgments C. Ohtsuki appreciates the financial support received from the Daiko Foundation, Nagoya, Japan.

References

1. Link S, El-Sayed MA. Spectral properties and relaxation dynamics of surface plasmon electronic oscillations in gold and silver nanodots and nanorods. J Phys Chem B. 1999;103:8410–26.
2. Kelly KL, Coronado E, Zhao LL, Schatz GC. The optical properties of metal nanoparticles: the influence of size, shape, and dielectric environment. J Phys Chem B. 2003;107:668–77.
3. Haes AJ, Van Duyne RP. A nanoscale optical biosensor: sensitivity and selectivity of an approach based on the localized surface plasmon resonance spectroscopy of triangular silver nanoparticles. J Am Chem Soc. 2002;124:10596–604.
4. Haes AJ, Van Duyne RP. A unified view of propagating and localized surface plasmon resonance biosensors. Anal Bioanal Chem. 2004;379:920–30.
5. Gorbunoff MJ. The interaction of proteins with hydroxyapatite. Anal Biochem. 1984;136:425–45.
6. Kawasaki T. Hydroxyapatite as a liquid chromatographic packing. J Chromatogr. 1991;544:147–84.
7. LeGeros RZ. Properties of osteoconductive biomaterials: calcium phosphates. Clin Orthop Relat Res. 2002;395:81–98.
8. Boyde A, Corsi A, Quarto R, Cancedda R, Bianco P. Osteoconduction in large macroporous hydroxyapatite ceramic implants: evidence for a complementary integration and disintegration mechanism. Bone. 1999;24:579–89.
9. Ichikawa Y, Ogata S, Torimoto T, Kawachi G, Kikuta K, Ohtsuki C. Hybridization of silver nanoparticles on hydroxyapatite in an aqueous solution. J Ceram Soc Japan. 2009;117:294–8.
10. Kawachi G, Watanabe T, Ogata S, Kamitakahara M, Ohtsuki C. Protein adsorption on needle-shaped hydroxyapatite prepared by hydrothermal treatment of mixture composed of $CaHPO_4 \cdot 2H_2O$ and β-$Ca_3(PO_4)_2$. J Ceram Soc Japan. 2009;117:847–50.
11. Ioku K, Kawachi G, Sasaki S, Fujimori H, Goto S. Hydrothermal preparation of tailored hydroxyapatite. J Mater Sci. 2006; 42:1341–4.
12. McFarland AD, Van Duyne RP. Single silver nanoparticles as real-time optical sensors with zeptomole sensitivity. Nano Lett. 2003;3:1057–62.
13. Zhang X, Bai R, Tong YW. Selective adsorption behaviors of proteins on polypyrrole-based adsorbents. Sep Purif Technol. 2006;52:161–9.